Prediction of dynamic behavior of workpieces in ultrasonic plastic welding

Takao HIRAI** Fumiyasu KURATANI** Tatsuya YOSHIDA** and Saiji WASHIO***

**Department of Mechanical Engineering, Graduate School of Engineering, University of Fukui,
3-9-1 Bunkyo, Fukui, 910-8507, Japan
E-mail: kuratani@mech.u-fukui.ac.jp
***Cybernet Systems Co., Ltd.,
1-3-8 Tokiwamachi, Chuo-ku, Osaka, 540-0028, Japan

Abstract

Ultrasonic plastic welding is a technique for joining thermoplastic parts through the use of frictional heat and deformation heat generated at the interface between the workpiece parts by high frequency mechanical vibration. This paper proposes a method for predicting the dynamic behavior of the contact surfaces of the parts at the beginning of the welding. The method is based on finite element dynamic contact analysis. To validate the proposed method, the predictions of dynamic behavior are compared with the measured data and a proper friction coefficient of the interface between the parts is determined. In addition, the dynamic behavior of the contact surfaces are investigated when the horn is vibrated at two different operating frequencies, 15 and 19 kHz. The results show that the dynamic behavior considerably depends on a friction coefficient. Furthermore, the displacements and elastic strains of the contact surfaces at 15 kHz are larger than those at 19 kHz. This seemingly results in the better quality of weld for 15 kHz operating frequency.

Key words: Ultrasonic Plastic Welding, Finite Element Analysis, Dynamic Contact Analysis, Friction

1. Introduction

Ultrasonic plastic welding is one of the most widely used techniques for joining thermoplastic parts in automobile, electronic and medical appliances. The technique does not require additional fasteners or adhesives and also the welding process is fast and efficient that consumes very little energy. In the welding process, high frequency mechanical vibration is applied to the parts to be joined through an ultrasonic horn. This generates heat due to friction and deformation of the contact surfaces and melts the plastics to accomplish the weld. The heat generation is very important for the quality of weld and is dependent on the dynamic behavior of the contact surfaces.

There are many studies on the design of ultrasonic horns[1]-[3]. These studies contribute to the saving energy consumption of ultrasonic welding. Several studies have been done on a model for the temperature distribution during welding[4],[5]. A few studies have been made on the effect of horn vibration on the properties of weld. Tsujino et al.[6],[7] measured the welding characteristics of plastic sheets when the horn is driven at the fundamental and several higher resonance frequencies simultaneously. This is an experimental investigation.

At the beginning of the welding, the contact surfaces of the workpiece parts being welded can come into contact and then separate, and also slide relative to each other. The interactions between the parts give a great influence on the dynamic behavior of the contact surfaces. To analyze its behavior that affects the heat generation, nonlinearity and transient effects must be considered in the analysis. For this, dynamic contact analysis is essential.

In this paper, we propose a method for predicting the dynamic behavior of the contact surfaces of the workpiece parts at the beginning of the welding. The method is based on finite element dynamic contact analysis. To validate the proposed method, the predictions of dynamic behavior are compared with the measured data. In addition, the effect of friction coefficient of the interface between the parts on the dynamic behavior is examined and a proper friction coefficient is determined. Furthermore, the displacements and elastic strains of the contact surfaces are investigated when the horn is vibrated at two different operating frequencies.

2. Ultrasonic plastic welding

Ultrasonic plastic welding is a technique for joining two thermoplastic parts together through the use of frictional heat and deformation heat generated by high frequency mechanical vibration.

Figure 1 shows an ultrasonic plastic welding. The workpiece parts considered in this paper are rotationally symmetric about the central axis except small ribs. The lengths of Part 1 and 2 are about 58 mm and about 31 mm. The location of the joint to be welded is about 7 mm from the bottom of horn. As a type of joint design, shear join is

chosen that is often used for joining round parts.

The basic process of ultrasonic plastic welding is as follows:
1. The two parts to be joined are placed one on top of the other on the fixture.
2. The horn is set into contact with the upper part and a controlled pressure is applied to the parts through the horn to hold them between the horn and fixture.
3. The horn is driven vertically at a frequency of 20 to 40 kHz and the vibrations are transmitted through the upper part to the joint interface.
4. Heat is generated due to friction and deformation of the contact surfaces and the heat melts the thermoplastics.
5. The contact surfaces are welded after the vibration is stopped to cool the melted plastic.
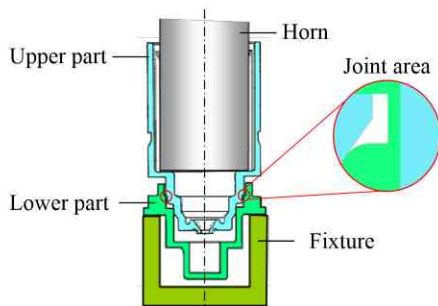

Fig. 1   Ultrasonic plastic welding

In the welding process, the heat generation is very important. Since the heat is generated due to friction and deformation of the contact surfaces, prediction and evaluation of the dynamic behavior such as friction and deformation are necessary. The dynamic behavior of the contact surfaces depends on both the dynamic characteristics of workpiece parts and the ultrasonic vibration of horn. On the other hand, the operating frequency of ultrasonic welding machine is usually fixed because the horn is driven at its resonant frequency.

We propose a method for predicting the dynamic behavior of the contact surfaces of the parts when the horn is driven at the operating frequency. The target of the method is the dynamic behavior at the beginning of the welding before their surfaces do not melt and plastically deform.

3. Welding experiment

In this paper, the dynamic behavior mean the displacement and elastic strain of the contact surfaces between the parts to be joined. Since in the welding experiment, there is a difficulty in directly measuring the displacement of the contact surfaces, the horizontal displacements were measured at Point A and B shown in Figure 2. The measured displacements are used to validate the method proposed for predicting the dynamic behavior.

Welding experiments were done at two different operating frequencies 15 and 19 kHz, and the laser displacement sensors (KEYENCE LK-G5000, 200 kHz sampling rate) were used.

The welding time is typically less than 1 s and the target dynamic behavior in this paper is at about 0.1 s after the horn vibration started. In the tensile test of the welded parts after the welding experiment, the quality of weld (tensile strength) for the 15 kHz operating frequency was better than that for the 19 kHz.
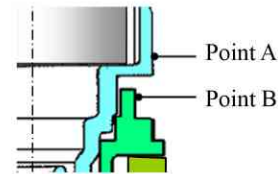

Fig. 2   Measuring point

4. Finite element analysis of contact problems

At the beginning of the welding, the surfaces of the workpiece parts being welded can come into and go out of contact with each other. To predict the dynamic behavior of the parts, we solve the dynamic contact problem that is highly nonlinear.

The basic steps for contact analysis using finite element (FE) software are as follows:
1. Build the FE models of the parts to be joined and the horn.
2. Identify the contact regions between the parts and between the upper part and horn.
3. Define contact elements by overlaying them on the contact regions.
4. Apply a sinusoidal displacement to the horn.
5. Solve the dynamic contact analysis.

Two surfaces that are already in contact or have a possibility of contact are called contact pairs. The FE model recognizes that the contact pairs are in contact or out of contact by the contact elements.

In contact problems, for the normal direction of the surface, two important are the forces transferred between parts and the impenetrability condition that one part cannot penetrate another part. Figure 3 shows the contact force and the impenetrability condition.
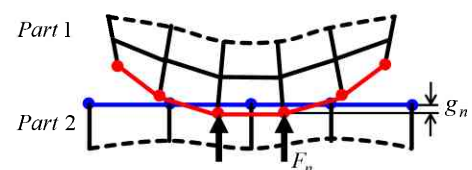

Fig. 3   Contact force and impenetrability condition

The impenetrability condition can be represented as

$$g_n = (\{u_1\} - \{u_2\}) \cdot \{n\} \geq 0 \qquad (1)$$

where g_n is the normal gap between the points on the surfaces of the parts for the contact pair, $\{u_1\}$ and $\{u_2\}$ are the position vectors of the points of Part 1 and 2, respectively and $\{n\}$ is the unit normal vector of the contact surface. If the contact pairs are in contact and violate the impenetrability condition, a contact algorithm is applied to satisfy the impenetrability condition. There are mainly three algorithms[8],[9]: penalty method, Lagrange multiplier method and augmented Lagrangian method.

Penalty method introduces a fictitious linear spring between contact pair shown in Figure 4 and the penetration can be controlled by the penalty parameter called the contact stiffness. The contact stiffness k_n affects both accuracy and convergency. As k_n is increased, the penetration g_n decreases, leading to very accurate results. On the other hand, high k_n can cause numerical instability because the stiffness matrix becomes ill condition. The contact force F_n is calculated by
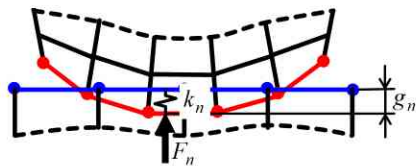
$$F_n = k_n g_n \qquad (2)$$

Fig. 4   Contact stiffness between contact pair

Lagrange multiplier method introduces Lagrange multiplier that is the contact force as an additional degree of freedom and solve for the contact force directly. Though this method provides an exact solution and does not need the contact stiffness, it has additional degrees of freedom and requires iterations to satisfy the impenetrability condition. This often causes ill converging.

Augmented Lagrangian method is a combination of the penalty and the Lagrangian multiplier methods. It starts with the penalty method and then if the penetration exceeds the allowable value, the contact force is augmented with Lagrange multiplier. The contact force is calculated by

$$F_n = k_n g_n + \lambda \qquad (3)$$

where λ is the Lagrange multiplier.

For the tangential direction of the surface, Coulomb's law is used to describe the friction phenomenon. The main problem with Coulomb friction law is the discontinuity of the friction force at transition from sticking to sliding. To permit a smooth transition from sticking to sliding, a model shown in Figure 5 is introduced. During sticking before sliding, a small deformation of parts is permitted. During sliding, the tangential force acting at the contact surfaces equals the friction force.
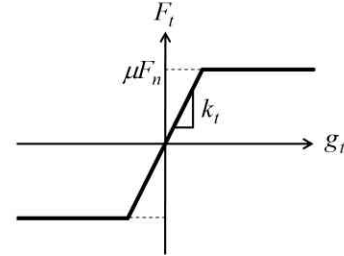

Fig. 5   Friction model

The tangential force F_t is calculated by

$$|F_t| = \begin{cases} k_t |g_t| & if \; |g_t| < \dfrac{\mu}{k_t} |F_n| & Sticking \\ \mu |F_n| & else & Sliding \end{cases} \qquad (4)$$

where k_t is tangential stiffness as penalty parameter, g_t is relative displacement along the tangential direction and μ is friction coefficient.

5. Dynamic contact analysis

In this paper, the finite element software ANSYS is used to perform dynamic contact analysis. The nonlinear contact problems are solved using the augmented Lagrangian method in the normal direction of the surface while the penalty method is used in the tangential direction. The implicit time integration algorithm is the Newmark method. In the analysis, the dynamic behavior of the contact surfaces are predicted when the horn is vibrated at two different operating frequencies and the difference in dynamic behavior is investigated.

5.1 Finite element model and analysis condition

Since both workpiece parts were rotationally symmetric about the central axis, an axisymmetric analysis was performed. Figure 6 shows the FE model of the workpiece parts being welded for contact analysis. The parts were modeled with two dimensional plane element (Plane182), the horn was defined as a rigid body. The material properties for the parts were: Young's modulus E=2.6 GPa, Poisson's ratio ν=0.35 and mass density ρ=1410 kg/m^3. The nodes on the interface between the lower part and fixture were constrained. Figure 7 shows the enlarged view of interfaces between the horn and the upper part, and between the two parts. The contact elements (Conta171 and Targe169) were overlaid on the surfaces. As the contact behavior between the contact elements (Conta171 and Targe169), separation to

the normal direction and sliding to the tangential direction were permitted.

In the contact analysis, first, the static amplitude of 40 μm was applied to the horn. Subsequently, the sinusoidal displacement was applied to the horn where the amplitude was 30 μm and frequency was 15 and 19 kHz that were the same as used in the experiments. The transient responses were calculated over 50 periods of each of the frequencies where the time step size is 1/200 of its period. The time step size and the contact stiffness were updated at each iteration to improve convergence. In addition, the material dependent beta damping was introduced: for 15 kHz, $\beta=1.7\times10^{-7}$ and for 19 kHz, $\beta=1.3\times10^{-7}$.
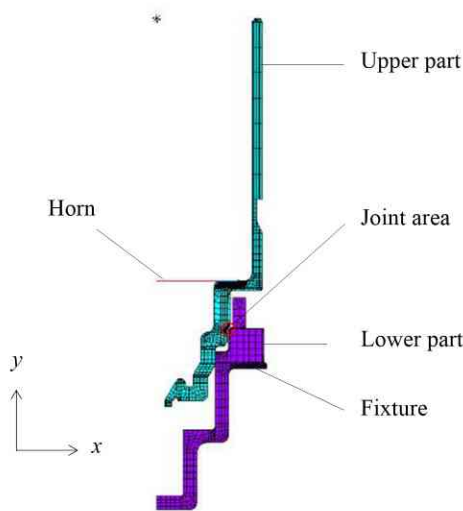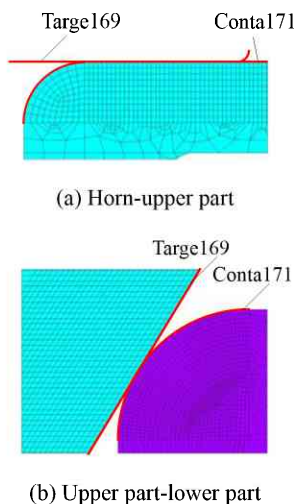

Fig. 6   FE model of the workpiece parts being welded

(a) Horn-upper part

(b) Upper part-lower part

Fig. 7   Contact surfaces

5.2 Effect of friction coefficient of the interface between the parts on the dynamic behavior

We examine the effect of friction coefficient of the

interface between the parts on the dynamic behavior of displacement and determine a proper friction coefficient. For this, the displacement responses were calculated for different friction coefficients, μ=0.2, 0.4 and 0.6. To determine a proper value of the friction coefficient, the predicted and the measured time data were transformed to frequency spectra and compared. This is because it is difficult to properly compare the predicted and measured displacement in the time domain.

Figure 8 shows the frequency spectra of displacements measured in the radial direction at point A and B shown in Figure 2. The frequency spectra were obtained from the time data at about 90 ms after the horn vibration started. Figure 8(a) is for the 15 kHz operating frequency and Figure 8(b) is for the 19 kHz operating frequency. For the 15 kHz, several large peaks are observed even though the horn is driven at 15 kHz. On the other hand, for the 19 kHz, there is a dominant peak at around 19 kHz.
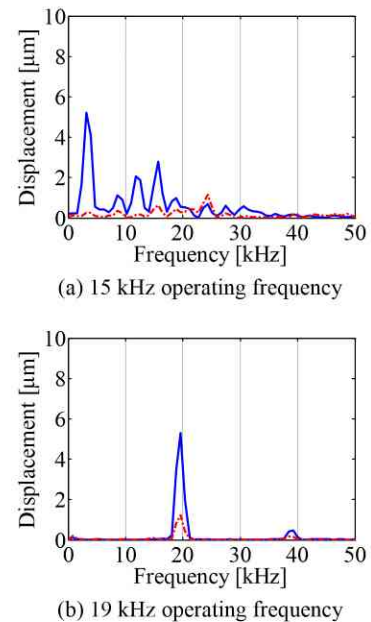

(a) 15 kHz operating frequency

(b) 19 kHz operating frequency

Fig. 8   Frequency spectrum (Experiment)
——— : Point A on the upper part   - - - : Point B on the lower part

Figures 9 and 10 show the frequency spectra of displacements calculated by the dynamic contact analysis. The time data were extracted from the calculated results at the nodes coincident with the measuring points in shown Figure 2. In the figures, (a) is for μ=0.2, (b) is for μ=0.4 and (c) is for μ=0.6, respectively.

From Figure 9 for the 15 kHz operating frequency, several large peaks are observed in each spectrum for all friction coefficients as in the experimental result and all three spectra have very similar distribution of peak frequencies. However, the peak value at around 18 kHz for μ=0.2 is very large compared to those for μ=0.4 and 0.6. This is slightly different from the experimental result.
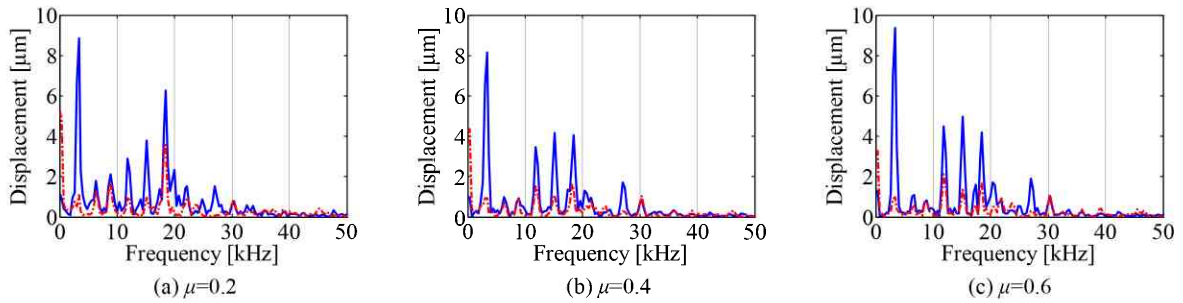
Fig. 9   Frequency spectrum (15 kHz operating frequency)
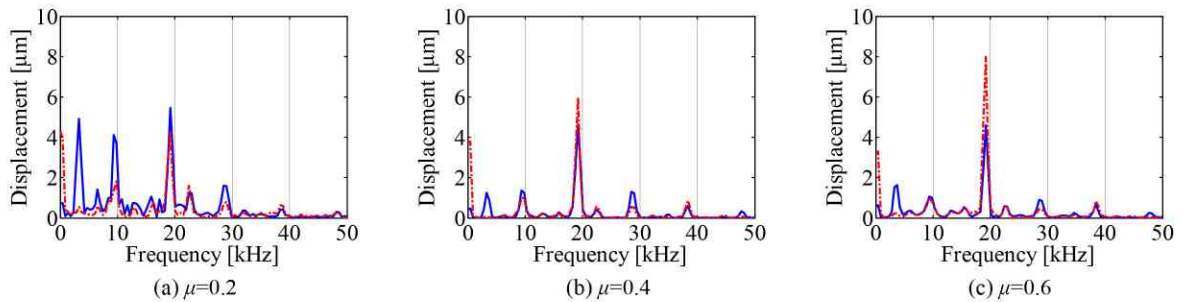——— : Point A on the upper part   - · - : Point B on the lower part

Fig. 10   Frequency spectrum (19 kHz operating frequency)
——— : Point A on the upper part   - · - : Point B on the lower part

From Figure 10 for the 19 kHz operating frequency, there is a significant difference in the number of large peaks when the spectra for three friction coefficients are compared. The spectrum of μ=0.2 has several large peaks while the spectra of μ=0.4 and 0.6 have a dominant peak at around 19 kHz. This is the same as in the measured result. Comparing the spectra of μ=0.4 and μ=0.6 indicates that the peak value of the lower part for μ=0.6 is larger than that for μ=0.4. This is clearly different from the experimental result. Thus the friction coefficient of the interface between the parts significantly affects the dynamic behavior of the parts, especially the behavior for the 19 kHz operating frequency.

Regarding a proper friction coefficient, the calculated behavior for μ=0.4 is close to the experimental one. We use μ=0.4 as the friction coefficient of the interface between the parts and investigate the dynamic behavior of the contact surfaces.

5.3 Dynamic behavior of the contact surfaces

We investigate the dynamic behavior of the contact surfaces based on the results obtained from the FE model with the friction coefficient μ=0.4. The nodes on the contact surfaces considered are shown in Figure 11.

Figures 12 and 13 show the time responses of displacements of the nodes for the operating frequency 15 and 19 kHz. In the figures, (a) is for the x direction (radial direction) and (b) is for the y direction (axial direction). Blue solid line indicates the upper part, red dashed dotted line indicates the lower part and black dashed line indicates the

horn. For the sake of reference, the displacement of horn in the y direction is depicted in the figures for the x direction. Note that the displacements are relative to the node positions shown in Figure 11(b) after the upper part was statically pressed by the horn.

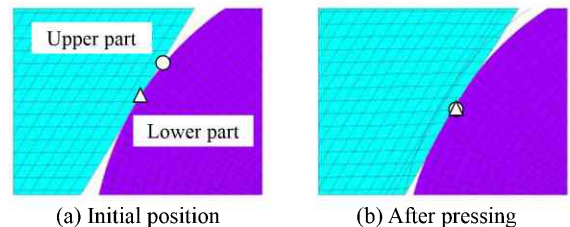(a) Initial position   (b) After pressing

Fig. 11   Movement of nodes after pressing

From Figure 12 for the 15 kHz operating frequency, the vibration displacements are not periodic even though the horn is vibrated at 15 kHz. In addition, the displacement of the upper part is much larger than that of the lower part and their displacements are out of phase with each other for both x and y direction. These imply that the upper part repeatedly comes into collision with the lower part at the interface. From Figure 13 for the 19 kHz operating frequency, the displacements of the parts are in phase with the horn for both x and y direction. This indicates that the two parts move synchronously with the horn and the parts slide relative to each other at the interface even though separation is permitted at the interface. Comparing the results of 15 and 19 kHz operating frequency indicates that the displacements

for the 15 kHz are larger than those for the 19 kHz, especially for the *y* direction (axial direction).
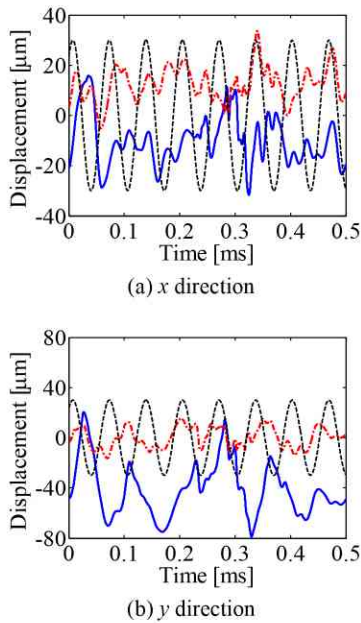

(a) *x* direction

(b) *y* direction

Fig. 12   Displacements of the contact surfaces
(15 kHz operating frequency)

—— : Upper part   – · – : Lower part   - - - : Horn

(a) *x* direction
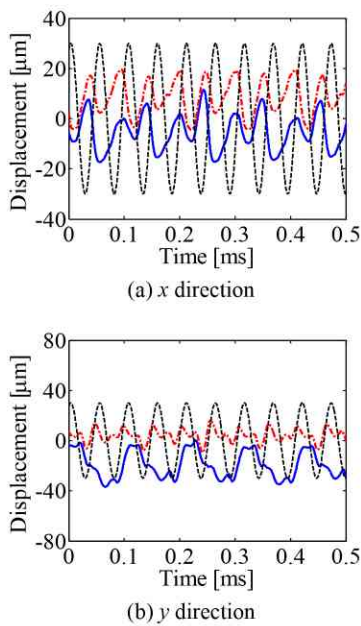

(b) *y* direction

Fig. 13   Displacements of the contact surfaces
(19 kHz operating frequency)

—— : Upper part   – · – : Lower part   - - - : Horn

5.4 Elastic strain of the contact surfaces

The heat generation depends on the deformation of the contact surfaces. We investigate the defamation based on the elastic strain on the contact surfaces shown in Figure 14 when the surfaces vibrate as shown in Figures 12 and 13.

Figure 15 shows the equivalent elastic strain obtained by the dynamic contact analysis. The horizontal axis denotes the element number on the surface and the vertical axis denotes the sum of the equivalent elastic strain at each time for each element.

The elastic strain for the 15 kHz is larger than that for the 19 kHz at all elements for both upper and lower parts. This is because the vibration displacements for the 15 kHz are large compared to those for the 19 kHz and the dynamic behavior for the 15 kHz demonstrates the collision phenomenon at the interface as shown in the previous section. Thus the 15 kHz operating frequency produces the large elastic strains due to the large displacements and the collision phenomenon at the interface. The large elastic strain leads to efficient heat generation due to the internal friction around the contact surfaces. This seemingly results in the difference in the quality of weld in the experiments between the 15 and 19 kHz operating frequency.
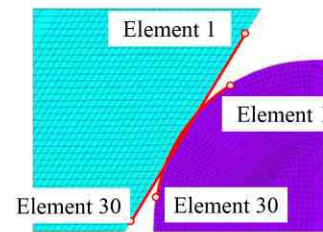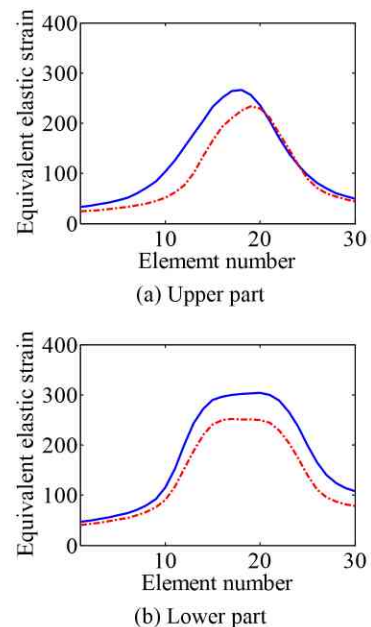

Fig. 14   Element number

(a) Upper part

(b) Lower part

Fig. 15   Equivalent elastic strain
—— : 15 kHz   – · – : 19 kHz

6. Conclusions

In this paper, we proposed the method for predicting the dynamic behavior of the contact surfaces of the workpiece

parts in the ultrasonic plastic welding. The method is based on the dynamic contact analysis. First, we examined the effect of friction coefficient on the dynamic behavior and determined the proper friction coefficient by comparing the predictions with the measured data. Next, we investigated the difference in dynamic behavior of the contact surfaces when the horn was vibrated at two different operating frequencies, 15 and 19 kHz. The results show that the friction coefficient of the interface significantly affects the dynamic behavior of the parts. The dynamic behavior for the 15 kHz operating frequency demonstrated that the upper part repeatedly comes into collision with the lower part at the interface and the displacements of the contact surfaces for 15 kHz are larger than those for 19 kHz. This produces the large equivalent elastic strains of the contact surfaces and seemingly results in the better quality of weld for 15 kHz operating frequency in the experiments.

References

(1) M. Naď, Ultrasonic horn design for ultrasonic machining technologies: Applied and Computational Mechanics, Volume 4(1), 2010, pp.79-88

(2) D.A. Wanga, W.Y. Chuang, K.Hsu, H.T. Pham, Design of a Bézier-profile horn for high displacement amplification, Ultrasonics, Volume 51, 2011, pp.148-156

(3) M. Roopa Rani and R. Rudramoorthy, Computational modeling and experimental studies of the dynamic performance, Ultrasonics, Volume 53, 2013, pp.763-772

(4) S. Elangovan, S. Semeer and K. Prakasan, Temperature and stress distribution in ultrasonic metal welding—An FEA-based study, Journal of materials processing technology, Volume 209, 2009, pp.1143-1150

(5) K.S. Suresh, M. Roopa Rani, K. Prakasan, R. Rudramoorthy, Modeling of temperature distribution in ultrasonic welding of thermoplastics for various joint designs, Journal of Materials Processing Technology, Volume 186, 2007, 138–146

(6) J. Tsujino, M. Hongoh, R. Tanaka, R. Onoguchi and T. Ueoka, Ultrasonic plastic welding using fundamental and higher resonance frequencies, Ultrasonics, Volume 40, 2002, pp.375-378

(7) J. Tsujino, M. Hongoh, M. Yoshikuni, H. Hashii, T. Ueoka, Welding characteristics of 27, 40 and 67 kHz ultrasonic plastic welding systems using fundamental and higher resonance frequencies, Ultrasonics, Volume 42, 2004, pp.131-137

(8) Ham-Ho Kim, Introduction to Nonlinear Finite Element Analysis, Springer, 2015, pp.367-426

(9) P. Wriggers, Finite Element Algorithms for Contact Problems, Archives of Computational Methods in Engineering, Volume 2(4), 1995, pp.1-49

Acknowledgements